ISSN 0915-633X

NATIONAL INSTITUTE FOR FUSION SCIENCE

Dependence of Au^- Production upon the Target Work Function in a Plasma-Sputter-Type Negative Ion Source

Y. Okabe, M. Sasao, H. Yamaoka, M. Wada
and J. Fujita

(Received – Apr. 9, 1991)

NIFS-85

May 1991

RESEARCH REPORT
NIFS Series

NAGOYA, JAPAN

Dependence of Au^- Production upon the Target Work Function in a Plasma-Sputter-Type Negative Ion Source

Yushirou OKABE, Mamiko SASAO, Hitoshi YAMAOKA[1], Motoi WADA[2] and Junji FUJITA

National Institute for Fusion Science, Nagoya 464-01

[1]The Institute of Physical and Chemical Research, Wako, Saitama 351-01

[2]Department of Electronics, Doshisha University, Kyoto, 602

Abstract

A method to measure the work function of the target surface in a plasma-sputter-type negative ion source has been developed. The present method can be used to determine the work function by measuring the photoelectric current induced by two lasers (He-Ne, Ar^+ laser). The dependence of Au^- production upon the work function of the target surface in the ion source was studied using this method. The time variation of the target work function and Au^- production rate were measured during the cesium coverage decrease due to the plasma ion sputtering. The observed minimum work function of a

cesiated gold surface in an Ar plasma was 1.3 eV where the negative ion production rate (Au^- current / target current) took the maximum value. The negative ion production rate showed the same dependence on the incident ion energy as that of the sputtering rate when the work function was constant.

KEYWORDS: Au^-, work function, plasma, negative ion source, photoelectric effect, ion source.

§1. Introduction

A plasma-sputter-type negative ion source, which was recently developed by Alton et al.[1] and Mori et al.[2], is very attractive not only for the application to a high-energy heavy ion accelerator, but also for that to a heavy ion beam for potential measurement of a magnetically confined plasma. Negative ions are formed on a target surface which is immersed in a plasma. The negative ion production rate at the target surface is supposed to be larger when the work function of the surface is lower. Therefore, alkali metals are usually deposited onto the target surface in order to reduce the work function, and to increase the negative ion production rate. However, the work function of the target changes drastically in a plasma due to sputtering by positive ions. Thus, a way to measure the work function of the target *in-situ* is needed in order to control the target surface condition and maintain a high negative ion production.

Wada studied the correlation of H^- production and the work function on a cesiated metal target in a hydrogen plasma of a self-extraction-type negative ion source by measuring the photoelectron emission threshold.[3] This method is based on Fowler's theory.[4] The work function of the target was successfully measured by minimizing the plasma noise and employing phase-sensitive detection. Although this method can determine the absolute value of the work function, it is not a convenient method to monitor the work function in a short period. The method requires a change of the wavelength of the incident light. A long integration time is also required to maintain a good signal-to-

noise ratio. A method that gives a quick measure of the work function is desirable, since the surface condition in a plasma often changes within a short period of time.

Yamaoka et al. have developed a simple method to monitor the surface condition with a good signal-to-noise ratio, by injecting a laser beam.[5] In this method relative yields of the measured photoelectric current are compared with the quantum yield calculated by Fowler's theory. They performed an experiment to measure the correlation of H^- production rates to the photoelectric current of a self-extraction= type negative ion source under various conditions.[5] This method is useful to monitor the rapid change of the surface condition with a small time constant, but the absolute value of the work function can't be accurately obtained. This is because the photoelectric current should be affected by the change in the absorptivity of photons at the surface.

In this paper, we describe a simple method to measure the work function of a target surface immersed in a plasma by injecting simultaneously two laser beams of different wavelengths. The absolute value of the work function is determined by comparing photoelectric currents at each wavelength. High power densities of laser lights make it possible to measure a rapid change in the surface work function without disturbing the plasma. By using this method, we measured the production rates of negative ions of gold (Au^-) in a plasma-sputter-type source under various conditions.

§2. Principle of the Work Function Measurement

As an example of a change in the work function due to alkali metal coverage, that of the Cs-Mo surface as a function of Cs thickness, quoted from Ph. D thesis by Wada, is shown in Fig. 1.[3] The work function of a bare Mo surface is 4.2 eV. By Cs adsorption, the work function falls from 4.2 eV to a minimum value of about 1.8 eV, and then increases again to 2.1 eV with further increasing Cs thickness. Near the work function minimum, the probability of forming negative ions is maximized. In the case of gold, the work function of a bare surface is 5.3 ~ 5.5 eV.[6] It is expected that the change in the work function for the Cs-Au system has the same tendency as that for the Cs-Mo system.

The basic theory of photoelectron emission from clean metals at various temperatures was studied by Fowler.[4] When the energy of the incident photon is close to the work function of a surface, the photon is absorbed by an electron near the surface and then the electron escapes from the metal with a kinetic energy corresponding to the difference between the potential energy and the incident photon energy. Here, the quantum efficiency Y is defined as the number of emitted electrons divided by the number of absorbed photons.

$$Y = \frac{(photoelectron\ number)}{(absorbed\ photon\ number)} \tag{1}$$

Electrons in the conduction band of the metal follow the

Fermi-Dirac statistics, and the number of electrons per unit volume, n, is given by the following formula:[4)]

$$n=\frac{4\sqrt{2}\,\pi\, m^{\frac{3}{2}} k^2 T^2 a}{h^3}\int_0^{\infty}\frac{\log\{1+\exp[-y+(h\nu-\Phi_w)/kT]\}}{\sqrt{y+(U_0-h\nu)/kT}}\,dy, \qquad (2)$$

where m is the electron mass, U_0 is the potential step at the boundary, $h\nu$ is the incident photon energy, Φ_w is the work function, and a is the absorptivity at the surface. In principle, the work function can be obtained by measuring the quantum efficiency of monochromatic light if U_0, a and T are known. However, in practice, it is not easy to measure the surface condition which changes drastically in a plasma.

The logarithm in eq. (2) is expanded and integrated term by term at the limit of $T \rightarrow 0$, and the first term gives the following formula for the quantum efficiency:

$$Y\propto\frac{a(h\nu-\Phi_w)^2}{(U_0-h\nu)^{\frac{1}{2}}}, \qquad h\nu>\Phi_w,$$

$$Y=0, \qquad h\nu<\Phi_w. \qquad (3)$$

When $h\nu=\Phi_w$, $Y\propto T^2$. If we assume a to be nearly constant, the square root of the quantum efficiency has an almost linear relationship with the work function. Here we must note that the theory is not a

good approximation at a higher value of μ, where $\mu = (h\nu - \Phi_w)/kT$. However, if the surface temperature is not too high compared with the room temperature, we can use the approximate formula (3) to determine the work function. For a wide range of the incident photon energy, eq. (2) should be used. In eq. (3), Y does not depend strongly on its denominator because the value of U_o is normally large (11 ~ 20 eV) compared with $h\nu$; therefore, Y depends mostly on the numerator.

When monochromatic laser light with the energy higher than the work function, the observed photoelectric current signal from the surface is a function of the work function. By using two different wavelength lasers simultaneously, two different photoelectric currents are obtained. The absolute value of the work function of a surface is calculated by the ratio of the value of these photoelectric currents:

$$\Phi_w = \frac{h\nu_1 - \zeta h\nu_2}{1-\zeta}, \qquad \zeta = \sqrt{\frac{(1-R_2)Y_1}{(1-R_1)Y_2}}. \tag{4}$$

Here, Y_1 and Y_2 are assumed to be proportional to the corresponding photoelectric current, and R_1 and R_2 ($R = 1 - a$) are reflectivities at each wavelength. The work function can be obtained by using relation (4) if the relative values of the quantum efficiencies and absorptivity at the two photon energies are measured.

§3. Experimental

3.1 *Ion source*

A schematic diagram of the experimental setup is shown in Fig. 2. The ion source consisting of a chamber of 10.8 cm in diameter and 12 cm long stainless steel vessel, was surrounded by eight columns of Sm-Co magnets in a multiline magnetic cusp geometry. A steady= state plasma was generated by primary electrons emitted from a 0.5 mm diameter tungsten filament. The entire chamber wall served as an anode for the discharge. A gold plate 0.5 mm thick and 2.3 cm in diameter was attached to a water-cooled Cu target by electron-beam welding, and was used as the sputter target (sputter probe) of the ion source.

By biasing the target negatively with respect to the plasma, positive ions from the plasma were accelerated across the sheath and struck the target surface. Negative ions of Au formed at the target surface were then accelerated back from the surface and measured by the beam diagnostic system.

A cesium oven was used to deposit cesium on the target. In order to control the cesium recycling from the wall, the chamber wall temperature was kept at around 60 °C.

The ion source was operated under the condition of the base pressure of 2.8×10^{-6} Torr. When the pressure of Ar reached about 1 mTorr, an argon arc plasma was produced.

3.2 *Work function measurement system*

In order to measure the work function of a cesiated target (gold in this case) in a plasma, two laser beams modulated to different frequencies were injected onto the target simultaneously and the induced photoelectric currents were detected with a phase-sensitive detection system tuned at each frequency. One was an Ar^+ laser (Coherent Innova 100) which oscillated at multiple frequencies, mainly 514.5 nm (2.41 eV) and 488 nm (2.54 eV) , and had a total output power of about 1 W. The other was a He-Ne laser which had a wavelength of 632.8 nm (1.96 eV), and an output power of 50 mW. Before the ion source operation, each laser power was measured on the target by power meters calibrated at each wavelength. The power of the Ar^+ laser measured on the target was 29.34 mW and that of the He-Ne laser was 1.67 mW. These laser beams were modulated by mechanical choppers to 263 Hz for the Ar^+ laser and 714 Hz for the He-Ne laser. These lasers were mixed into one beam, and collimated on the same spot on the target.

During the operation of the source, the target was usually biased at V_t = - 200 V, and the typical target current was around I_t = 1 ~ 2 mA. Photoelectric currents induced by these two laser beams were less than 10^{-4} times the target current. The phase-sensitive method made the detection of the photoelectric current at a high S / N ratio possible. The induced photoelectric current was separated from the plasma noise by using two lock-in amplifiers tuned at the frequency of

modulation for each laser beam, and the outputs are connected to a multiparameter recorder system.

A portion of each laser beam is reflected by the optical glass before it passes the chopper system to monitor the injected power. The measured powers are also recorded on the recorder, as well as are other ion source variables such as the arc current, the target current, and the target temperature.

3.3 *Detection system for* Au^-

All species of negative ions produced in a plasma-sputter-type negative ion source have an initial energy corresponding to the target voltage. Therefore, masses of negative ion species from the source can be analyzed by a magnetic momentum analyzer located downstream of the beam. Without cesium introduction, the beam was dominated by impurity components such as $C_2H_2^-$. Once the cesium vapor was introduced, they disappeared and a peak corresponding to Au^- appeared. A movable Faraday cup (F. C.) at the upstream was set and the vertical profile of the beam and time-dependent correlation to photoelectric currents were measured. In the shield box of the movable F. C., a pair of permanent magnets were installed as well as an electron dump of graphite. A negative ion beam collimated by the entrance aperture of 3 mm diameter passed through the magnetic field, but electrons were deflected by the magnetic field. Therefore, only negative ions were detected by the F. C. Another weak magnetic field was also applied to suppress the secondary electrons from the faraday

cup. The details of the F. C. system were described in ref. 7. The detected current of Au^- was also recorded on the multiparameter recorder.

The retarding potential-type electrostatic analyzer (E. S. A.) which moved in the direction perpendicular to the Au^- ion beam was used for the measurement of the energy spread of a negative ion beam. Because of the spatial restriction, F. C. and E. S. A. were not used at the same time. The experimental results of the measurement of the energy spread of Au^- ion beam obtained with this E. S. A. will be published elsewhere.

§4. Results and Discussion

4.1 *Measurement of laser light absorptivity*

To observe the influence of the condition of the gold surface on the absorptivity of laser light of the surface, the ratio of an injected laser power to a reflected light power on the gold target in the ion source was measured. An injected laser light passed through an injection port and was reflected on a gold target surface. A reflected light was monitored by a 2.5 cm diameter power meter after it passed through an exit port. The laser light was injected at 45° with respect to the target surface. The incident photon energies were 1.96 eV for He-Ne laser, 2.40, 2.47, 2.52, 2.54, and 2.61 eV for Ar^+ laser, respectively. Two surface conditions, (1) smooth as-received sample, and (2) rough after a mechanical treatment with emery, were tested.

The measured dependence of the reflectivity upon the incident photon energy is shown in Fig. 3. The reflectivity decreased for a higher incident photon energy. For an as-received gold surface, the value was higher than that of a polished one. This difference was caused mainly by the diffuse reflection on a polished gold surface. The following experiments were performed with the polished gold surface.

The reflectivity of a cesium-covered gold surface was also measured during the source operation. It was typically 24 % for He-Ne laser and 8 % for Ar^+ laser.

4.2 *Two-wavelength measurement of photoelectric current*

Cesium introduction was terminated but a small amount of cesium was still deposited on the target surface due to the recycling from the wall of the ion source. Then the time evolution of the photoelectric current induced by the Ar^+ laser and the He-Ne laser, the corresponding monitored laser powers, the target current, and the Au^- current was measured during the source operation. To see the process wherein the work function of the target surface was changed by the decrease of cesium coverage caused by Ar^+ sputtering, the time variation of these variables was monitored simultaneously. The Ar plasma was operated under the conditions of an arc power of I_d = 61 mA, V_d = 45 V, a target voltage V_t = - 200 V and a gas pressure of 1 mTorr.

The target current and monitored laser powers were nearly

constant but two photoelectric currents decreased with time. From two photoelectric currents, the time-dependence of the work function was obtained by using eq. (4). Here, the change in the reflectivity of each laser light due to the cesium deposition was taken into account.

From the integration of the measured vertical profile of the beam, the total Au^- current was estimated to be 400 times the detected Au^- current, assuming the beam was cylindrically symmetric. The correlation between the negative ion production rate and the work function is shown in Fig. 5. Here the negative ion production rate was defined to be Au^- current / target current. The discharge conditions were as follows: Ar 1 mTorr, V_d = 45 V, I_d = 61 mA, V_t = - 200 V. The highest Φ_w obtained in this experiment was 1.89 eV. The Φ_w of the gold surface in an Ar plasma with weak cesium introduction was reported to decrease to 1.5 eV, utilizing two different wavelength lasers alternately without correcting the absorptivity.[8] In the present experiment, the negative ion production rate monotonically decreased for increasing target work function from 1.34 to 1.89 eV. The negative ion production rate was 3.2 % (Au^- current = 40.7 μA, target current, I_t = 1.28 mA) when the target work function was 1.34 eV.

The electron tunneling model proposed by Yu predicts the relation of the negative ion yield to the work function,[9] as below:

$$Y = AY_0 \frac{16E(V_1+\Delta\varphi)}{V_0^2} \exp[-2(\frac{2m}{\hbar^2})^{\frac{1}{2}}(V_1+\Delta\varphi)^{\frac{1}{2}}b], \quad (5)$$

where A is the neutralization probability of the ion by the tunneling of an electron between the ion and the substrate, Y_0 is the total sputtering yield, E is the energy of the electron, V_0 is the height of the tunneling barrier, V_1 is the initial barrier of the potential when there is no Cs, $\Delta\varphi$ is the work function change, and b is the potential width. If we assume the initial barrier of the potential and the potential width as those fitted to H^-, D^-, and Mo^- data, then the Au^- production rate would change by a factor of 3 ~ 11 for the change of 0.5 eV in this work function region. However, our observation indicated change of only a factor of two. This deviation was considered to be due to (1) saturation of negative ion production rate at a low Φ_w region, as Yu showed in the case of $^{16}O^-$, or (2) suppression of sputtering of gold atoms due to high cesium coverage on the target surface. The error was within $\pm$ 4 % for the Au^- production rate and that in determining the work function was within $\pm$ 20 % considering the scattering of the data signals caused by the plasma noise.

4.3 *Au^- production under the constant Φ_w condition*

Figure 6 shows the effect of discharge current on the Au^- production rate. The discharge conditions were Ar 1 mTorr, V_d = 45 V, and V_t = - 200 V, and Φ_w was kept at 1.3 eV, which was the lowest Φ_w value observed. Under the constant Φ_w condition, both the target current and the Au^- current was proportional to the discharge current. Then the negative ion production rate, estimated to be 3.4 %,

was not found to depend on the discharge current. The error was within ± 4 % for the Au^- production rate and within ± 1 % for discharge current. The main error was the scatter of the data signals caused by the plasma noise.

The effect of the target voltage on the Au^- production was studied under the constant work function condition, as shown in Fig. 7. The solid line is the calculated sputtering yield.[10] The experimental conditions were the following: Ar 1 mTorr and $V_d = 45$ V, and Φ_w was kept at 1.8 eV. The negative ion production rate increased as the target voltage increased. This tendency is qualitatively similar to the calculated sputtering yield curve. This suggests that the increased negative ion production rate is simply due to the enhanced sputtering yield through high energy beam.

§5. Conclusion

A method to measure the work function of a target surface in a negative ion source during source operation has been developed. The method was able to determine the work function as a function of time by measuring photoelectric currents induced by a He-Ne laser (632.8 nm) and an Ar^+ laser (488 nm) simultaneously. In this experiment, the reflectivity at each wavelength on a cesiated gold surface in an Ar plasma was measured and was taken into account in determining the work function of a cesiated gold surface. The dependence of Au^- production upon the target work function of a

plasma-sputter-type negative ion source was studied using this method.

The work function of a clean gold surface is known to be 5.3 ~ 5.5 eV.[6] By introducing cesium on the gold surface, it was decreased down to 1.3 eV. The negative ion production rate (Au^- current / target current) monotonically decreased to a half as the target work function increased from 1.34 to 1.89 eV (Fig. 5). This work function dependence of Au^- production did not fit the theoretical prediction proposed by Yu.[9] This deviation was considered to be due to the fact, (1) that the production rate of Au^- was saturated or (2) that the gold surface to be sputtered was covered by cesium. The maximum Au^- current density on the target (Au^- current / target surface area) was 9.2 $\mu A / cm^2$ when the cesiated target work function, discharge current and discharge voltage were 1.34 eV, 61 mA, and -200 V, respectively.

Under the constant work function of a cesiated gold surface in an Ar plasma, both the Au^- current and the target current increased in proportion to the discharge current in the discharge current range investigated. This fact corresponds to the constant negative ion production efficiency of 3.4 % (Fig. 6).

The negative ion production rate (Au^- current / target current) increased as the target voltage increased from 100 to 200 V when the work function was the same (1.8 eV). This tendency was qualitatively similar to the reported sputtering yield curve.[10]

Acknowledgements

This work was performed under the Collaborating Research Program of the National Institute for Fusion Science, and was partly supported by the Grant-in-Aid for Scientific Research from the Ministry of Education, Science and Culture.

References

1) G. D. Alton, Y. Mori, A. Takagi, A. Ueno and S. Fukumoto: Nucl. Instrum. & Methods. **A270** (1988) 194.

2) Y. Mori, G. D. Alton, A. Takagi, A. Ueno and S. Fukumoto: Nucl. Instrum. & Methods. **A273** (1988) 5.

3) M. Wada: Ph. D. Thesis, LBL-Report 15800, Lawrence Berkeley Laboratory, Univ. California, Berkeley (1983).

4) R. H. Fowler: Phys. Rev. **38** (1931) 45.

5) H. Yamaoka, M. Sasao, M. Wada and H. J. Ramos: Nucl. Instrum. & Methods. **B36** (1989) 277.

6) H. C. Patter and J. M. Blakely: J. Vac. Sci. & Technol. **12** (1975) 635.

7) K. N. Leung, K. W. Ehlers and M. Bacal: Rev. Sci. Instrum. **54** (1983) 56.

8) M. Sasao, Y. Okabe, J. Fujita, M. Wada and H. Yamaoka: Rev. Sci. Instrum. **61-1** (1990) 418.

9) M. L. Yu: Phys. Rev. Lett. **40** (1978) 574.

10) N. Matsunami, Y. Yamamura, K. Itikawa, N. Itoh, Y. Kazumata, S. Miyagawa, K. Morita, R. Shimizu and H. Tawara: At. Data and Nucl. Data Tables, **31** (1984) 75.

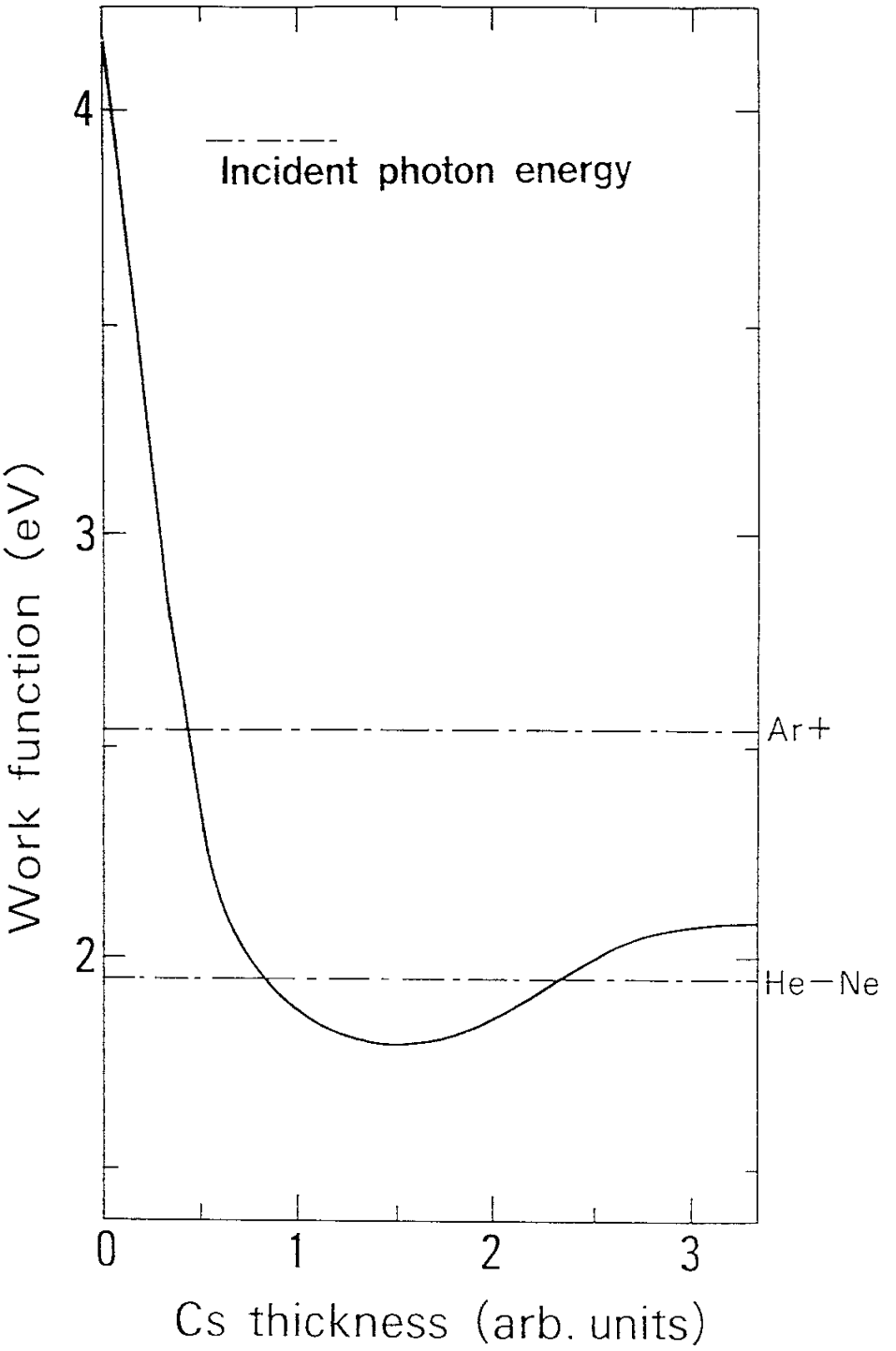

Fig. 1. Change in the work function of Mo covered with Cs (ref. 3).

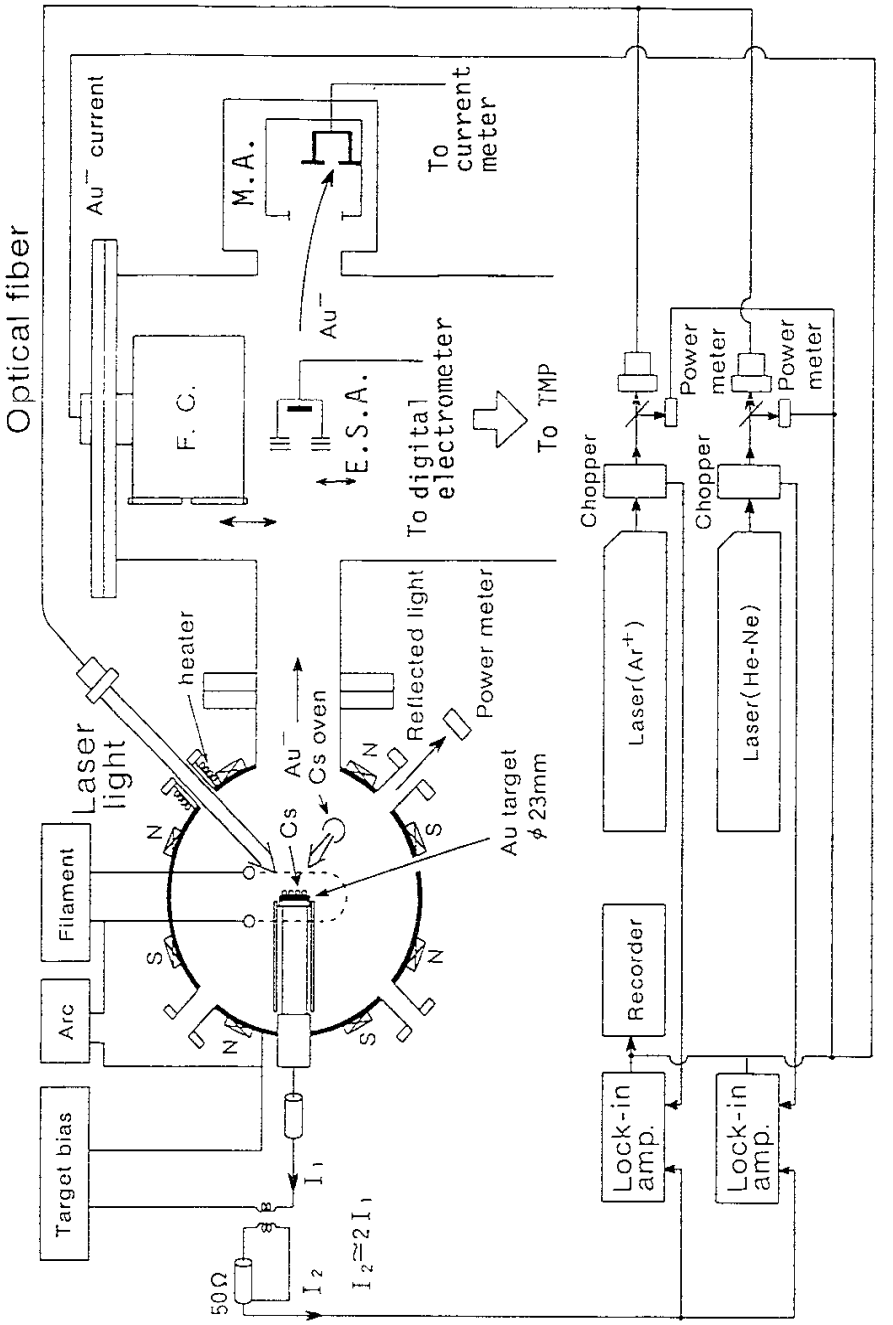

Fig. 2. Schematic diagram of the experimental setup.

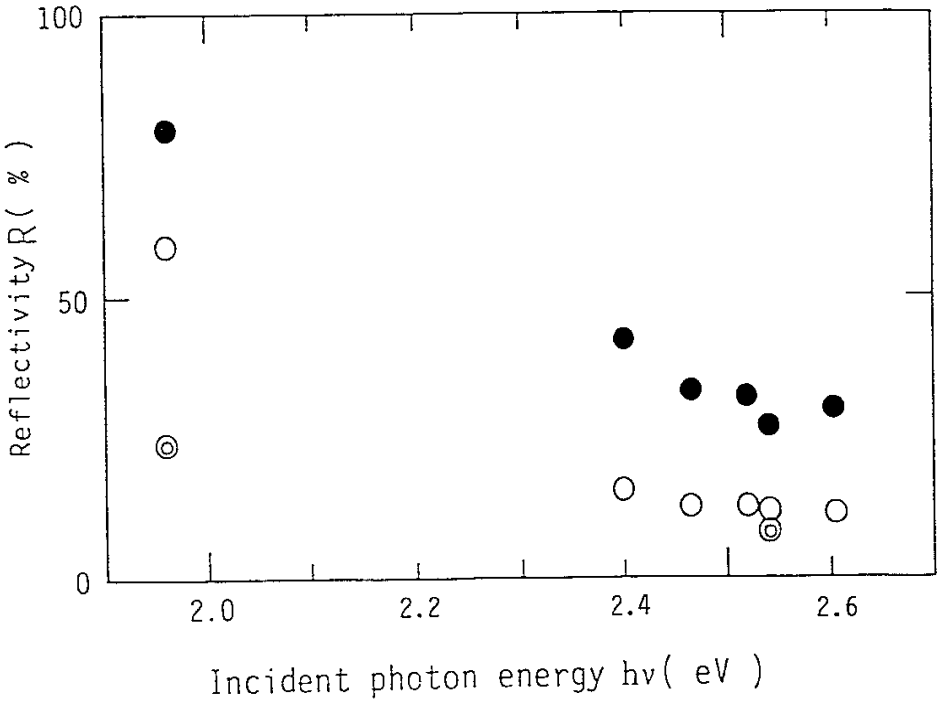

Fig. 3. Change in the reflectivity of gold surface for the different wavelengths of laser light and the different roughnesses of the surface. ●: as-received, ○: after mechanical treatment with emery, ◎: in Ar plasma with cesium; the experimental conditions were the following: Ar 1mTorr, V_d = 45 V, I_d = 61 mA, V_t = - 200 V.

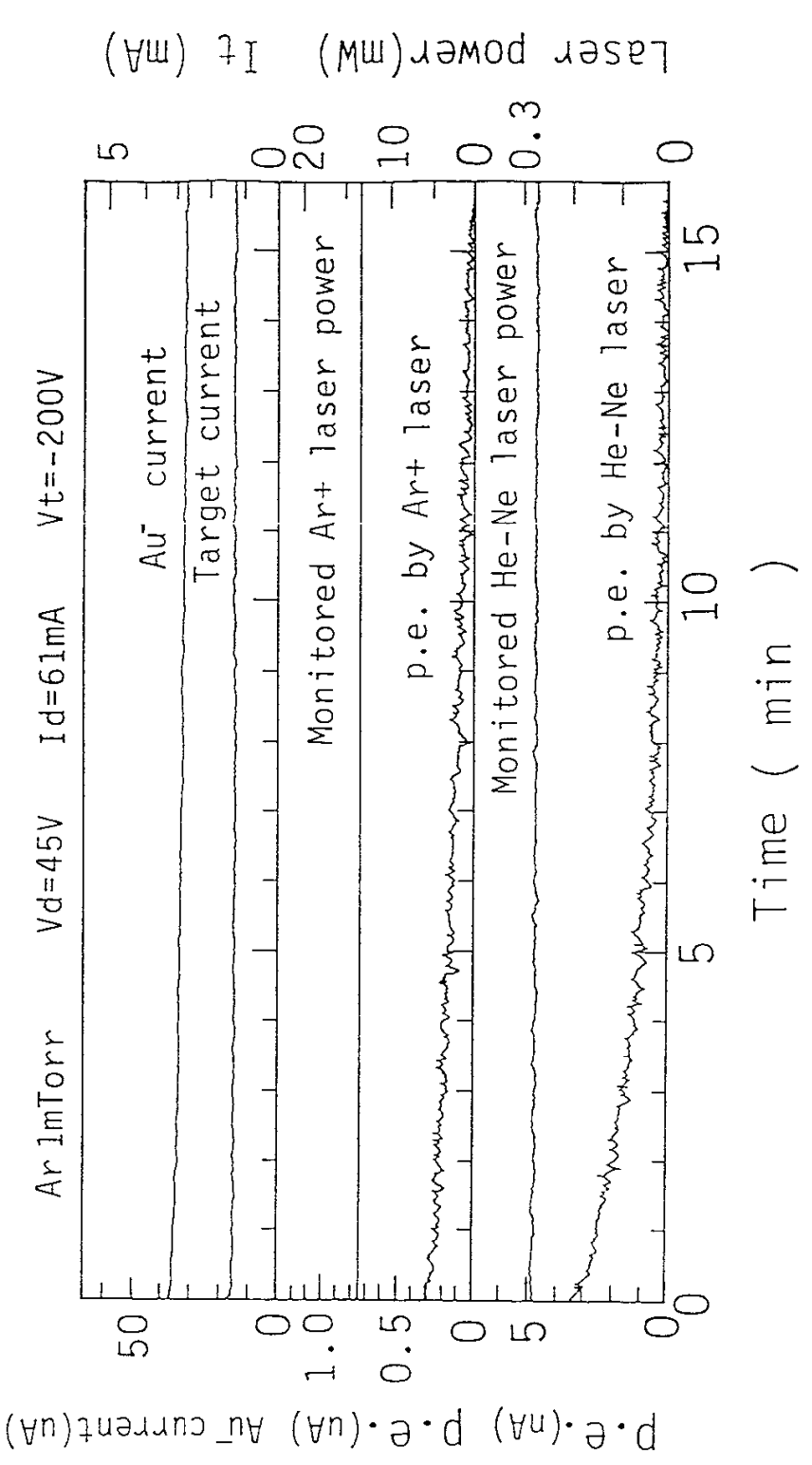

Fig. 4. Time-dependent signal of photoelectric currents *p. e*, (He-Ne, Ar^+), Au^- current, monitored laser power and target current. The experimental conditions were the following: Ar 1 mTorr, V_d = 45 V, I_d = 61 mA, V_t = - 200 V.

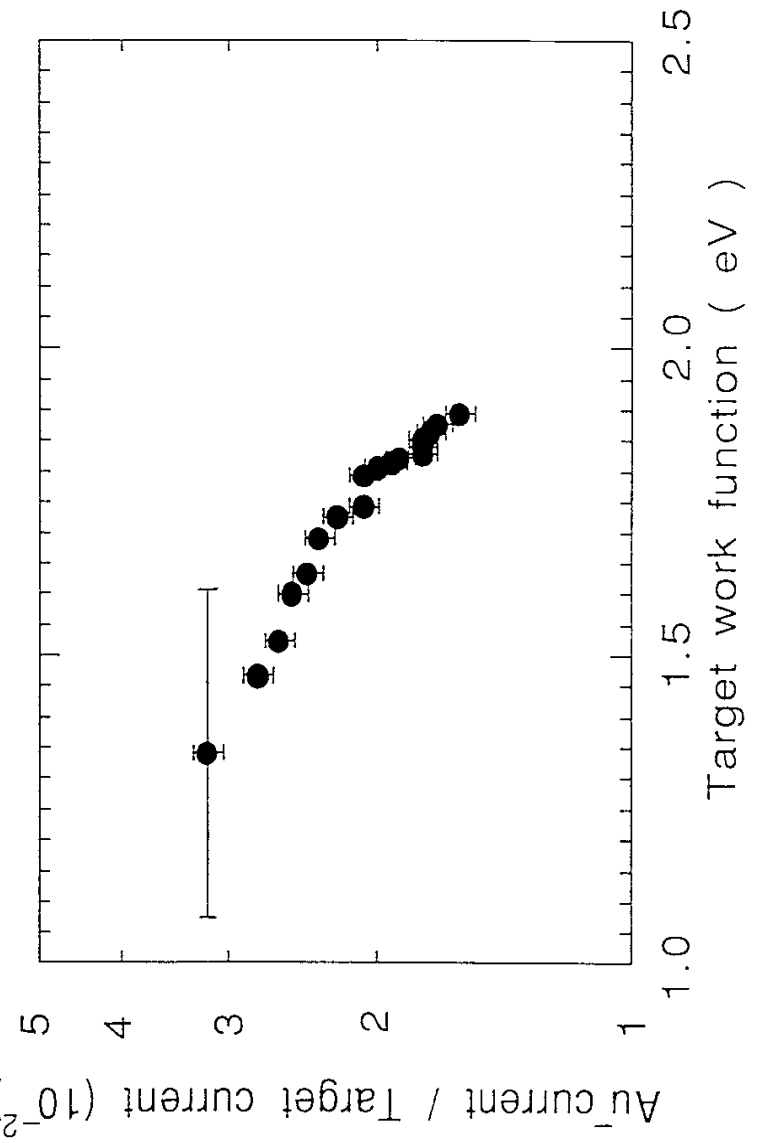

Fig. 5. Correlation between the measured work function and the Au^- production rate. The production rate is defined as the ratio of the extracted Au^- current to the target current. The experimental conditions were the same as shown in Fig. 4.

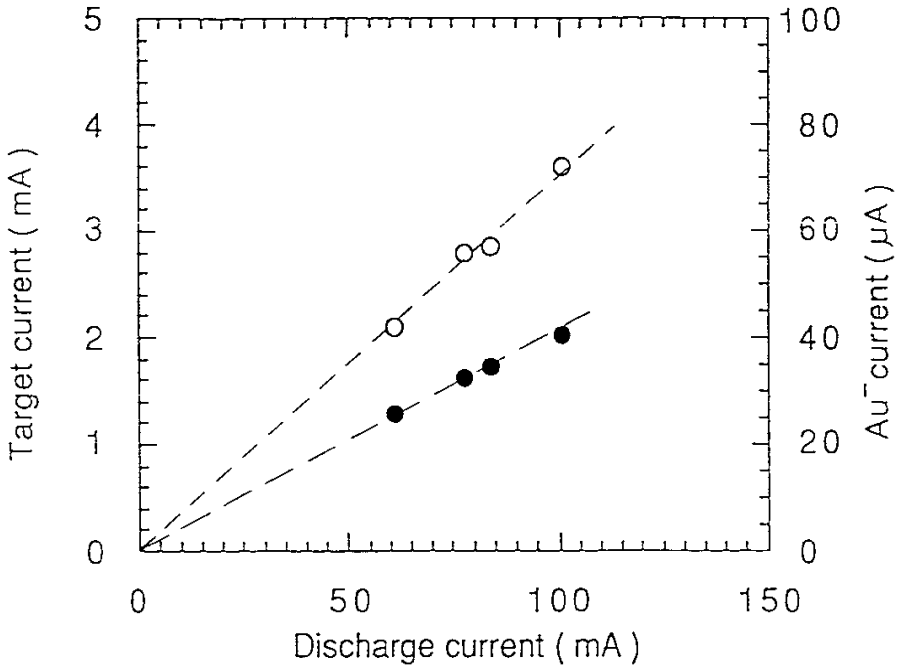

Fig. 6. Effect of the discharge current on the Au^- production rate under the constant work function 1.3 eV and Ar 1 mTorr discharge, V_d = 45 V, V_t = - 200 V. O: Au^- current, ●: Target current.

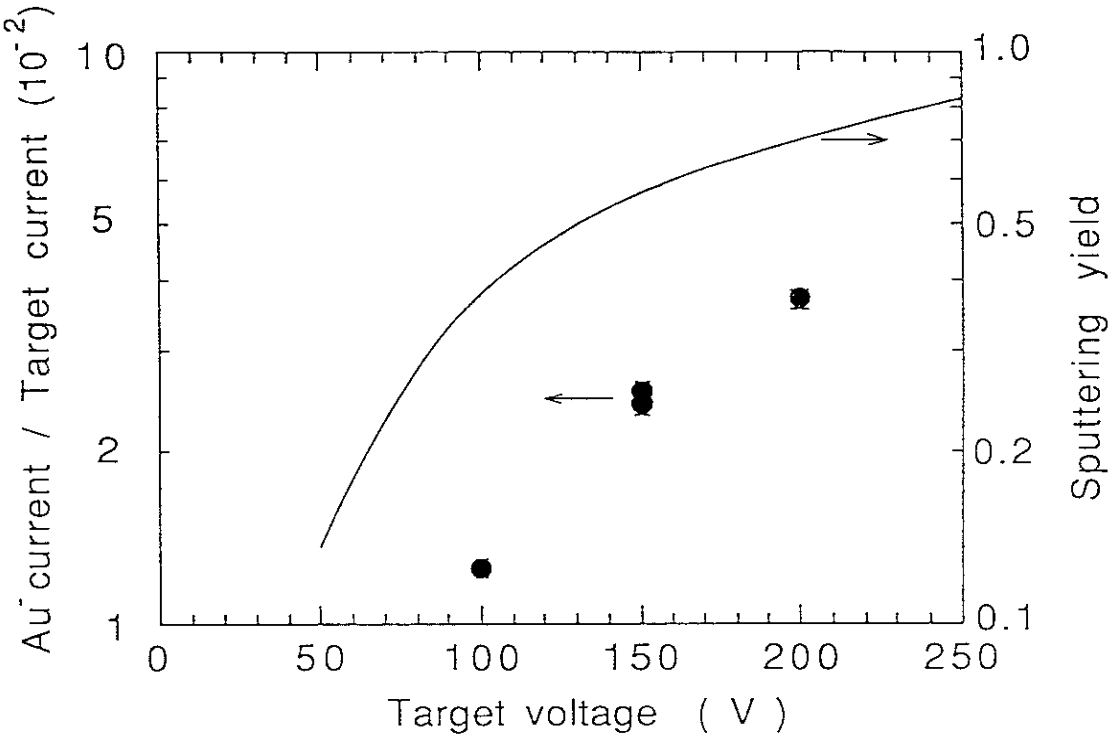

Fig. 7. Effect of target voltage on the Au^- production rate under the constant work function 1.8 eV and Ar 1 mTorr discharge, V_d = 45 V, V_t = - 200 V. The solid curve represents the sputtering yield.

Recent Issues of NIFS Series

NIFS-32 Yoshi H. Ichikawa, *Experiments and Applications of Soliton Physics*; June 1990

NIFS-33 S.-I. Itoh, *Anomalous Viscosity due to Drift Wave Turbulence* ; June 1990

NIFS-34 K. Hamamatsu, A. Fukuyama, S.-I. Itoh, K. Itoh and M. Azumi, *RF Helicity Injection and Current Drive* ; July 1990

NIFS-35 M. Sasao, H. Yamaoka, M. Wada and J. Fujita, *Direct Extraction of a Na- Beam from a Sodium Plasma* ; July 1990

NIFS-36 N. Ueda, S.-I. Itoh, M. Tanaka and K. Itoh, *A Design Method of Divertor in Tokamak Reactors* Aug. 1990

NIFS-37 J. Todoroki, *Theory of Longitudinal Adiabatic Invariant in the Helical Torus*; Aug. 1990

NIFS-38 S.-I. Itoh and K. Itoh, *Modelling of Improved Confinements – Peaked Profile Modes and H-Mode–* ; Sep. 1990

NIFS-39 O. Kaneko, S. Kubo, K. Nishimura, T. Syoji, M. Hosokawa, K. Ida, H. Idei, H. Iguchi, K. Matsuoka, S. Morita, N. Noda, S. Okamura, T. Ozaki, A. Sagara, H. Sanuki, C. Takahashi, Y. Takeiri, Y. Takita, K. Tsuzuki, H. Yamada, T. Amano, A. Ando, M. Fujiwara, K. Hanatani, A. Karita, T. Kohmoto, A. Komori, K. Masai, T. Morisaki, O. Motojima, N. Nakajima, Y. Oka, M. Okamoto, S. Sobhanian and J. Todoroki, *Confinement Characteristics of High Power Heated Plasma in CHS*; Sep. 1990

NIFS-40 K. Toi, Y. Hamada, K. Kawahata, T. Watari, A. Ando, K. Ida, S. Morita, R. Kumazawa, Y. Oka, K. Masai, M. Sakamoto, K. Adati, R. Akiyama, S. Hidekuma, S. Hirokura, O. Kaneko, A. Karita, T. Kawamoto, Y. Kawasumi, M. Kojima, T. Kuroda, K. Narihara, Y. Ogawa, K. Ohkubo, S. Okajima, T. Ozaki, M. Sasao, K. Sato, K.N. Sato, T. Seki, F. Shimpo, H. Takahashi, S. Tanahashi, Y. Taniguchi and T. Tsuzuki, *Study of Limiter H- and IOC- Modes by Control of Edge Magnetic Shear and Gas Puffing in the JIPP T-IIU Tokamak*; Sep. 1990

NIFS-41 K. Ida, K. Itoh, S.-I. Itoh, S. Hidekuma and JIPP T-IIU & CHS Group, *Comparison of Toroidal/Poloidal Rotation in CHS Heliotron/Torsatron and JIPP T-IIU Tokamak*; Sep .1990

NIFS-42 T.Watari, R.Kumazawa,T.Seki, A.Ando,Y.Oka, O.Kaneko, K.Adati, R.Ando, T.Aoki, R.Akiyama, Y.Hamada, S.Hidekuma, S.Hirokura, E.Kako, A.Karita, K.Kawahata, T.Kawamoto, Y.Kawasumi, S.Kitagawa, Y.Kitoh, M.Kojima, T. Kuroda, K.Masai, S.Morita, K.Narihara, Y.Ogawa, K.Ohkubo, S.Okajima, T.Ozaki, M.Sakamoto, M.Sasao, K.Sato, K.N.Sato, F.Shinbo, H.Takahashi, S.Tanahashi, Y.Taniguchi, K.Toi, T.Tsuzuki, Y.Takase, K.Yoshioka, S.Kinoshita, M.Abe, H.Fukumoto,

K.Takeuchi, T.Okazaki and M.Ohtuka, *,Application of Intermediate Frequency Range Fast Wave to JIPP T-IIU and HT-2 Plasma*; Sep. 1990

NIFS-43 K.Yamazaki, N.Ohyabu, M.Okamoto, T.Amano, J.Todoroki, Y.Ogawa, N.Nakajima, H.Akao, M.Asao, J.Fujita, Y.Hamada, T.Hayashi, T.Kamimura, H.Kaneko, T.Kuroda, S.Morimoto, N.Noda, T.Obiki, H.Sanuki, T.Sato, T.Satow, M.Wakatani, T.Watanabe, J.Yamamoto, O.Motojima, M.Fujiwara, A.Iiyoshi and LHD Design Group, *Physics Studies on Helical Confinement Configurations with l=2 Continuous Coil Systems*; Sep. 1990

NIFS-44 T.Hayashi, A.Takei, N.Ohyabu, T.Sato, M.Wakatani, H.Sugama, M.Yagi, K.Watanabe, B.G.Hong and W.Horton, *Equilibrium Beta Limit and Anomalous Transport Studies of Helical Systems*; Sep. 1990

NIFS-45 R.Horiuchi, T.Sato, and M.Tanaka, *Three-Dimensional Particle Simulation Study on Stabilization of the FRC Tilting Instability*; Sep. 1990

NIFS-46 K.Kusano, T.Tamano and T. Sato, *Simulation Study of Nonlinear Dynamics in Reversed-Field Pinch Configuration*; Sep. 1990

NIFS-47 Yoshi H.Ichikawa, *Solitons and Chaos in Plasma*; Sep. 1990

NIFS-48 T.Seki, R.Kumazawa, Y.Takase, A.Fukuyama, T.Watari, A.Ando, Y.Oka, O.Kaneko, K.Adati, R.Akiyama, R.Ando, T.Aoki, Y.Hamada, S.Hidekuma, S.Hirokura, K.Ida, K.Itoh, S.-I.Itoh, E.Kako, A. Karita, K.Kawahata, T.Kawamoto, Y.Kawasumi, S.Kitagawa, Y.Kitoh, M.Kojima, T.Kuroda, K.Masai, S.Morita, K.Narihara, Y.Ogawa, K.Ohkubo, S.Okajima, T.Ozaki, M.Sakamoto, M.Sasao, K.Sato, K.N.Sato, F.Shinbo, H.Takahashi, S.Tanahashi, Y.Taniguchi, K.Toi and T.Tsuzuki, *Application of Intermediate Frequency Range Fast Wave to JIPP T-IIU Plasma*; Sep.1990

NIFS-49 A.Kageyama, K.Watanabe and T.Sato, *Global Simulation of the Magnetosphere with a Long Tail: The Formation and Ejection of Plasmoids*; Sep.1990

NIFS-50 S.Koide, *3-Dimensional Simulation of Dynamo Effect of Reversed Field Pinch*; Sep. 1990

NIFS-51 O.Motojima, K. Akaishi, M.Asao, K.Fujii, J.Fujita, T.Hino, Y.Hamada, H.Kaneko, S.Kitagawa, Y.Kubota, T.Kuroda, T.Mito, S.Morimoto, N.Noda, Y.Ogawa, I.Ohtake, N.Ohyabu, A.Sagara, T. Satow, K.Takahata, M.Takeo, S.Tanahashi, T.Tsuzuki, S.Yamada, J.Yamamoto, K.Yamazaki, N.Yanagi, H.Yonezu, M.Fujiwara, A.Iiyoshi and LHD Design Group, *Engineering Design Study of Superconducting Large Helical Device*; Sep. 1990

NIFS-52 T.Sato, R.Horiuchi, K. Watanabe, T. Hayashi and K.Kusano, *Self-Organizing Magnetohydrodynamic Plasma*; Sep. 1990

NIFS-53 M.Okamoto and N.Nakajima, *Bootstrap Currents in Stellarators and Tokamaks*; Sep. 1990

NIFS-54 K.Itoh and S.-I.Itoh, *Peaked-Density Profile Mode and Improved Confinement in Helical Systems*; Oct. 1990

NIFS-55 Y.Ueda, T.Enomoto and H.B.Stewart, *Chaotic Transients and Fractal Structures Governing Coupled Swing Dynamics*; Oct. 1990

NIFS-56 H.B.Stewart and Y.Ueda, *Catastrophes with Indeterminate Outcome*; Oct. 1990

NIFS-57 S.-I.Itoh, H.Maeda and Y.Miura, *Improved Modes and the Evaluation of Confinement Improvement*; Oct. 1990

NIFS-58 H.Maeda and S.-I.Itoh, *The Significance of Medium- or Small-size Devices in Fusion Research*; Oct. 1990

NIFS-59 A.Fukuyama, S.-I.Itoh, K.Itoh, K.Hamamatsu, V.S.Chan, S.C.Chiu, R.L.Miller and T.Ohkawa, *Nonresonant Current Drive by RF Helicity Injection*; Oct. 1990

NIFS-60 K.Ida, H.Yamada, H.Iguchi, S.Hidekuma, H.Sanuki, K.Yamazaki and CHS Group, *Electric Field Profile of CHS Heliotron/Torsatron Plasma with Tangential Neutral Beam Injection*; Oct. 1990

NIFS-61 T.Yabe and H.Hoshino, *Two- and Three-Dimensional Behavior of Rayleigh-Taylor and Kelvin-Helmholz Instabilities*; Oct. 1990

NIFS-62 H.B. Stewart, *Application of Fixed Point Theory to Chaotic Attractors of Forced Oscillators;* Nov. 1990

NIFS-63 K.Konn., M.Mituhashi, Yoshi H.Ichikawa,*Soliton on Thin Vortex Filament;* Dec. 1990

NIFS-64 K.Itoh, S.-I.Itoh and A.Fukuyama,*Impact of Improved Confinement on Fusion Research;* Dec. 1990

NIFS -65 A.Fukuyama, S.-I.Itoh and K. Itoh,*A Consistency Analysis on the Tokamak Reactor Plasmas;* Dec. 1990

NIFS-66 K.Itoh, H. Sanuki, S.-I. Itoh and K. Tani,*Effect of Radial Electric Field on α-Particle Loss in Tokamaks;* Dec. 1990

NIFS-67 K.Sato,and F.Miyawaki,*Effects of a Nonuniform Open Magnetic Field on the Plasma Presheath*; Jan.1991

NIFS-68 K.Itoh and S.-I.Itoh,*On Relation between Local Transport Coefficient and Global Confinement Scaling Law;* Jan. 1991

NIFS-69 T.Kato, K.Masai, T.Fujimoto,F.Koike, E.Källne, E.S.Marmar and J.E.Rice,*He-like Spectra Through Charge Exchange Processes in Tokamak Plasmas;* Jan.1991

NIFS-70 K. Ida, H. Yamada, H. Iguchi, K. Itoh and CHS Group, *Observation of Parallel Viscosity in the CHS Heliotron/Torsatron* ; Jan.1991

NIFS-71 H. Kaneko, *Spectral Analysis of the Heliotron Field with the Toroidal Harmonic Function in a Study of the Structure of Built-in Divertor* ; Jan. 1991

NIFS-72 S. -I. Itoh, H. Sanuki and K. Itoh, *Effect of Electric Field Inhomogeneities on Drift Wave Instabilities and Anomalous Transport* ; Jan. 1991

NIFS-73 Y.Nomura, Yoshi.H.Ichikawa and W.Horton,*Stabilities of Regular Motion in the Relativistic Standard Map;* Feb. 1991

NIFS-74 T.Yamagishi, *;Electrostatic Drift Mode in Toroidal Plasma with Minority Energetic Particles,* Feb. 1991

NIFS-75 T.Yamagishi, *Effect of Energetic Particle Distribution on Bounce Resonance Excitation of the Ideal Ballooning Mode,* Feb. 1991

NIFS-76 T.Hayashi, A.Takei, N.Ohybu, T.Sato, *Suppression of Magnetic Surface Breaking by Simple Extra Coils in Finite Beta Equilibrium of Helical System*; Feb. 1991

NIFS-77 N.Ohyabu, *High Temperature Divertor Plasma Operation;* Feb. 1991

NIFS-78 K.Kusano, T.Tamano and T.Sato, *Simulation Study of Toroidal Phase-Locking Mechanism in Reversed-Field Pinch Plasma;* Feb. 1991

NIFS-79 K.Nagasaki, K.Itoh and S.-I.Itoh, *Model of Divertor Biasing and Control of Scrape-off Layer and Divertor Plasmas;* Feb. 1991

NIFS-80 K.Nagasaki and K.Itoh, *Decay Process of a Magnetic Island by Forced Reconnection;* Mar. 1991

NIFS-81 K.Takahata, N.Yanagi, T.Mito, J.Yamamoto, O.Motojima and LHD Design Group, K.Nakamoto, S.Mizukami, K.Kitamura, Y.Wachi, H.Shinohara, K.Yamamoto, M.Shibui, T.Uchida and K.Nakayama, *Design and Fabrication of Forced-Flow Coils as R&D Program for Large Helical Device*; Mar 1991

NIFS-82 T.Aoki and T.Yabe,*Multi-dimensional Cubic Interpolation for ICF Hydrodynamics Simulation*; Apr.1991

NIFS-83 K.Ida, S.-I.Itoh, K.Itoh, S.Hidekuma, Y.Miura, H.Kawashima, M.Mori, T.Matsuda, N.Suzuki, H.Tamai, T.Yamauchi and JFT-2M Group,*Density Peaking in the JFT-2M Tokamak Plasma with Counter Neutral Beam Injection;*May.1991

NIFS-84 A.Iiyoshi,*Development of the Stellarator/Heliotron Research*;May.1991